Publication dates:

January, April, July and October.

Subscription rates:

Rs. 24.00 for India

$ 6 50 for U.S.A.

£ 2-25 for U.K.

Equivalent of Rs. 30.00 for other countries.

Subscriptions are accepted only on volume basis.

Enquiries regarding subscriptions and exchange may be addressed to:

MR. T. K. S. IYENGAR
Associate Editor
Journal of the
Indian Institute of Science
Bangalore-12, (India).

[Publishes original research carried out in the various Departments of the Institute.]

JOURNAL OF
THE INDIAN INSTITUTE OF SCIENCE

Volume 54] **Number 1** **[January 1972**

CONTENTS

PAGE

JOURNAL OF

THE

INDIAN INSTITUTE OF SCIENCE

Volume 54

1972

INDIAN INSTITUTE OF SCIENCE
BANGALORE 12
INDIA

Journal of the Indian Institute of Science
Vol. 54, No. 1, January 1972

STUDY OF THE SURFACE WAVE AND RADIATION CHARACTERISTICS OF CYLINDRICAL METALLIC CORRUGATED STRUCTURES*

By (MISS) H. M. GIRIJA AND S. K. CHATTERJEE
(*Indian Institute of Science, Bangalore-12*)

[Received : September 2, 1971]

ABSTRACT

Surface wave characteristics like the guide wavelength, radial field decay, and radiation characteristics of a corrugated circular cylindrical metal rod are verified experimentally. A comparative study of the surface wave characteristics of the corrugated line, Sommerfeld surface wave line Harms-Goubau line reveal that corrugated structure compares favourably with the Harms-Goubau line and is superior to Sommerfeld line.

1. INTRODUCTION

The object is to present experimental results on the surface wave and radiation characteristics of a uniformly corrugated conductor excited in E_0-mode and to verify some of the results of the theory published elsewhere[1, 2] by the authors.

2. CORRUGATED STRUCTURES

The corrugated structures (See Fig. 1,) used for experiment have the following specifications (Table 1).

3. RADIAL FIELD DECAY

The radial field decay (See Fig. 2) was measured by using a monopole probe. Some of the results are reported in Figures 3-5. The results show good agreement with theory. The theoretical value of the radial field component E_ρ of the fundamental harmonic is given by[1]

$$E_\rho = C_0 \frac{\beta_0}{\gamma_0} H_1^{(1)} (j\gamma_0 \rho) \exp(-j\beta_0 z) \qquad [1]$$

In Figs. 3-5 the normalisation of E_ρ is made with respect to the field amplitude at a distance of 1 mm from the structure. The axial propagation

*The work is supported by PL—480 contract No. E—262—69 (N).

constant β_0 and radial propagation constant γ_0 for the fundamental harmonic are determined from the relations

$$\frac{2k_0}{l}\,\frac{J_0(\beta_0 W/2)\sin(\beta_0 W/2)}{\beta_0} = -\gamma_0\,\frac{K_0(\gamma_0 b)}{K_1(\gamma_0 b)}\,\frac{F_1(k_0 b)}{F_0(k_0 b)}\,. \qquad [2]$$

and

$$\beta_0^2 = \gamma_0^2 + k_0^2 \qquad [3]$$

where,

$$F_0(k_0 b) = J_0(k_0 a)\,Y_0(k_0 b) - Y_0(k_0 a)\,J_0(k_0 b) \qquad [4]$$

and

$$F_1(k_0 b) = J_0(k_0 a)\,Y_1(k_0 b) - Y_0(k_0 a)\,J_1(k_0 b) \qquad [5]$$

TABLE 1.

Specifications of the structure dimensions.

a = inner rod radius = 0·25 cm. b = disc radius in cms.

$l - W$ = thickness of discs = 0·047 cm. l = period of the structure.

W = disc spacing in cms. L = length of the structure = 75 cm.

Structure Number	b (cms.)	W (cms.)	Structure Number	b (cms.)	W (cms.)
1	0·4	0·2	8	0·5	0·2
2	0·4	0·4	9	0·5	0·4
3	0·4	0·6	10	0·5	0·6
4	0·4	0·8	11	0·5	0·8
5	0·4	1·0	12	0·5	1·0
6	0·4	1·2	13	0·5	1·2
7	0·4	1·4	14	0·5	1·4

4. GUIDE WAVELENGTH

The guide wavelength is measured from the plot of E_ρ *Vs* z_A. The measured values of λ_g as a function of spacing are compared with the theoretical values of λ_g calculated from the relation $\lambda_g = 2\lambda/\beta_0$, (See fig. 6). The measured values of λ_g for the structures are tabulated below.

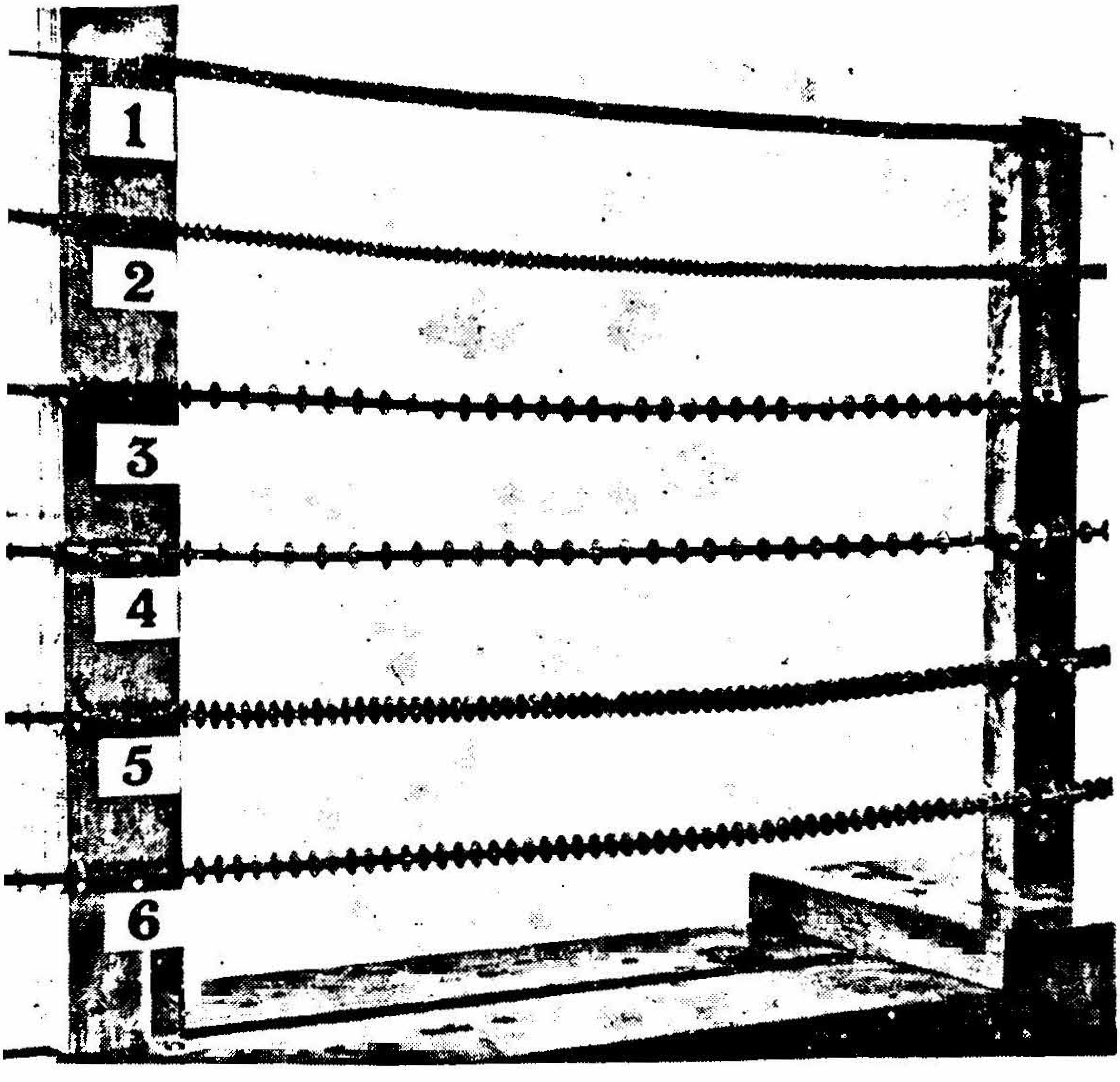

FIG. 1

Surface wave structures

constant β_0 and radial propagation constant γ_0 for the fundamental harmonic are determined from the relations

$$\frac{2k_0}{l}\frac{J_0(\beta_0 W/2)\sin(\beta_0 W/2)}{\beta_0} = -\gamma_0 \frac{K_0(\gamma_0 b)}{K_1(\gamma_0 b)}\frac{F_1(k_0 b)}{F_0(k_0 b)}. \tag{2}$$

and

$$\beta_0^2 = \gamma_0^2 + k_0^2 \tag{3}$$

where,

$$F_0(k_0 b) = J_0(k_0 a)\,Y_0(k_0 b) - Y_0(k_0 a)\,J_0(k_0 b) \tag{4}$$

and

$$F_1(k_0 b) = J_0(k_0 a)\,Y_1(k_0 b) - Y_0(k_0 a)\,J_1(k_0 b) \tag{5}$$

TABLE 1.

Specifications of the structure dimensions.

a = inner rod radius = 0·25 cm. b = disc radius in cms.
$l-W$ = thickness of discs = 0·047 cm. l = period of the structure.
W = disc spacing in cms. L = length of the structure = 75 cm.

Structure Number	b (cms.)	W (cms.)	Structure Number	b (cms.)	W (cms.)
1	0·4	0·2	8	0·5	0·2
2	0·4	0·4	9	0·5	0·4
3	0·4	0·6	10	0·5	0·6
4	0·4	0·8	11	0·5	0·8
5	0·4	1·0	12	0·5	1·0
6	0·4	1·2	13	0·5	1·2
7	0·4	1·4	14	0·5	1·4

4. GUIDE WAVELENGTH

The guide wavelength is measured from the plot of E_ρ Vs z_A. The measured values of λ_g as a function of spacing are compared with the theoretical values of λ_g calculated from the relation $\lambda_g = 2\lambda/\beta_0$. (See fig. 6). The measured values of λ_g for the structures are tabulated below.

TABLE 2

Measured values of guide wavelength λ_g (cms).
Free space wavelength λ_0=3.2 cms.

Structure Number*	λ_g (cms.)	Structure Number*	λ_g (cms.)
1	2·72	8	2·4
2	2·85	9	2·45
3	2·96	10	2·6
4	2·29	11	2·65
5	3·13	12	2·77
6	3·06	13	2·89
7	2·98	14	3·0

*Refer to Table 1 for values of *b* and *W*.

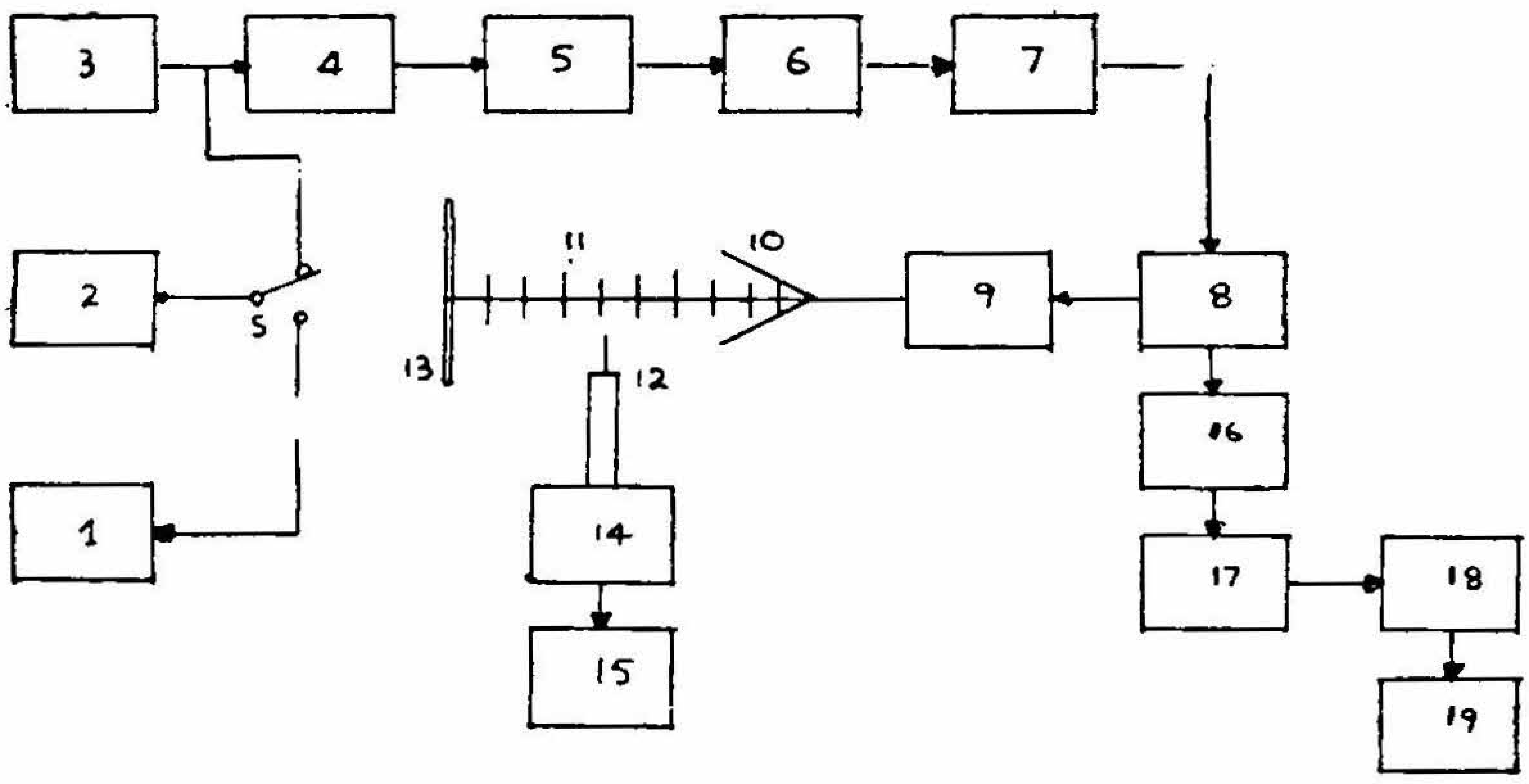

FIG. 2

Block schematic diagram of the experimentai set-up for surfacə wave field measurement.

1. Saw tooth generator
2. Square wave modulator
3. Klystron power supply
4. Klystron (723 A/B) and feed
5. ' Uniline ' ferrite isolator (CRC Model 88-96 B)
6. Precision frequency meter (PRD Type 55 B-A)
7. Precision attenuator (PRD Type 115-B)
8. H-Tee (PRD type 461)
9. Wave guid to cozial adapter (Micro line model 249)
10. Circular metal cane
11. Cylindrical corrugated strucher
12. Monopole probe
13. Aluminium plate terminating the structur
14. Caystal tuner (PRD type 612 A)
15. Detector amplifier
16. Flap attenuator (PRD type 160)
17. Waveguide tuner (PRD type 302)
18. Detecting section
19. Detector amplifier

S. Switch for applying saw tooth or square wave to the reflector of the klystron

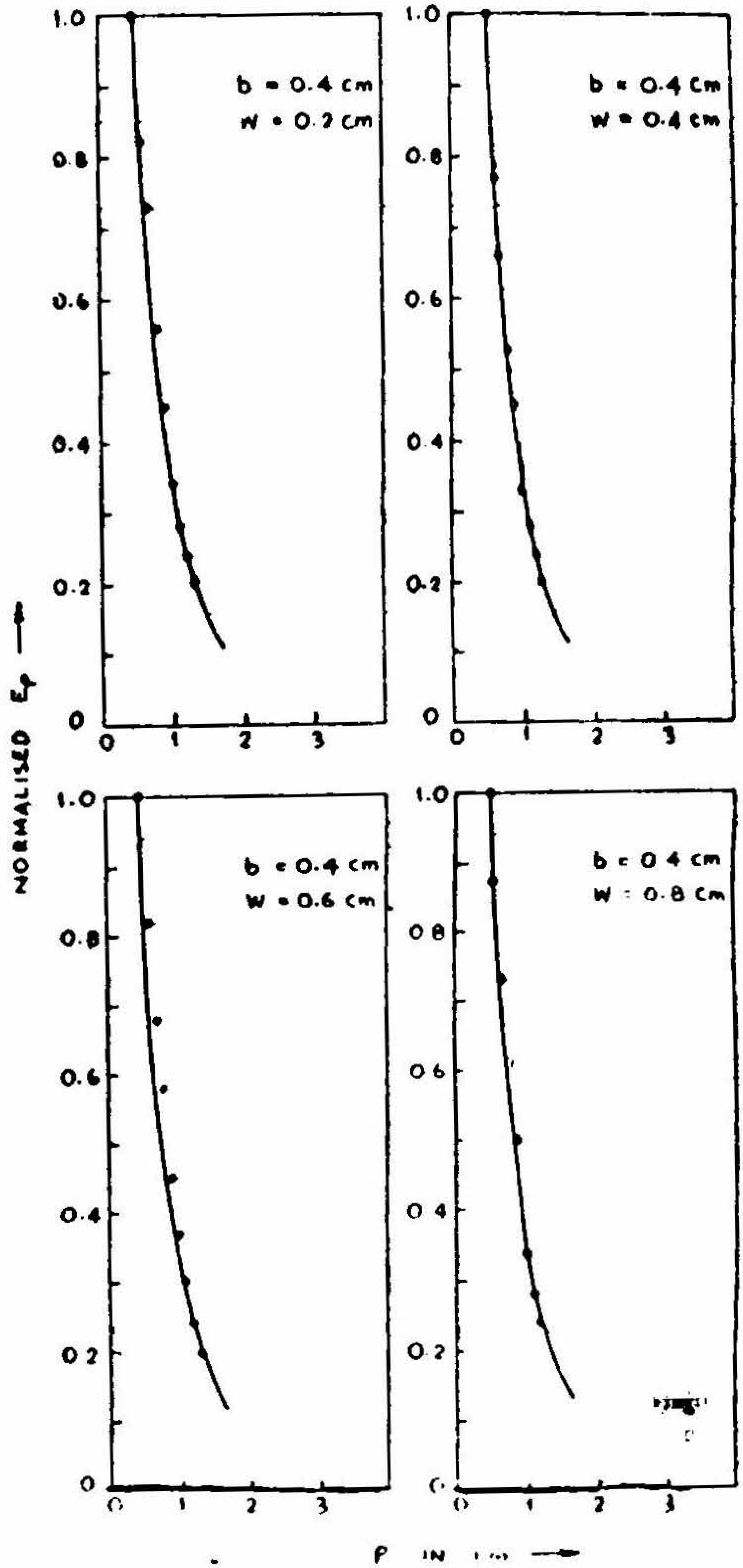

FIG. 3

Experimental and theoretical plots for the component E_ρ

b : Disc-radius — Theoretical graph

w : Disc-spacing . . Experimental points

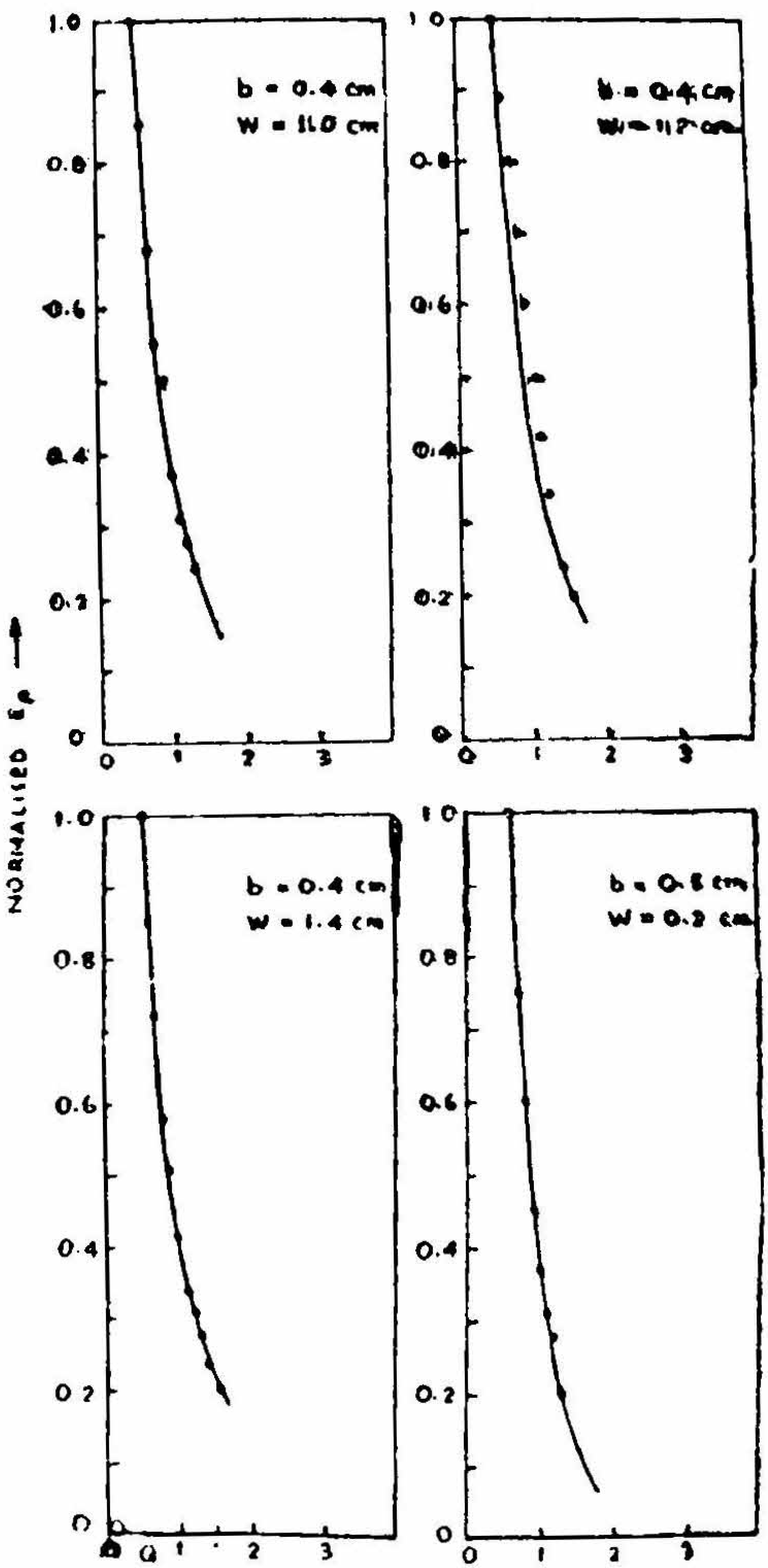

FIG. 4

Experimental and theoretical slots fcr the component E_ρ

b : Disc-radius —— Theoretical graph

w : Disc-spacing · · Experimental points

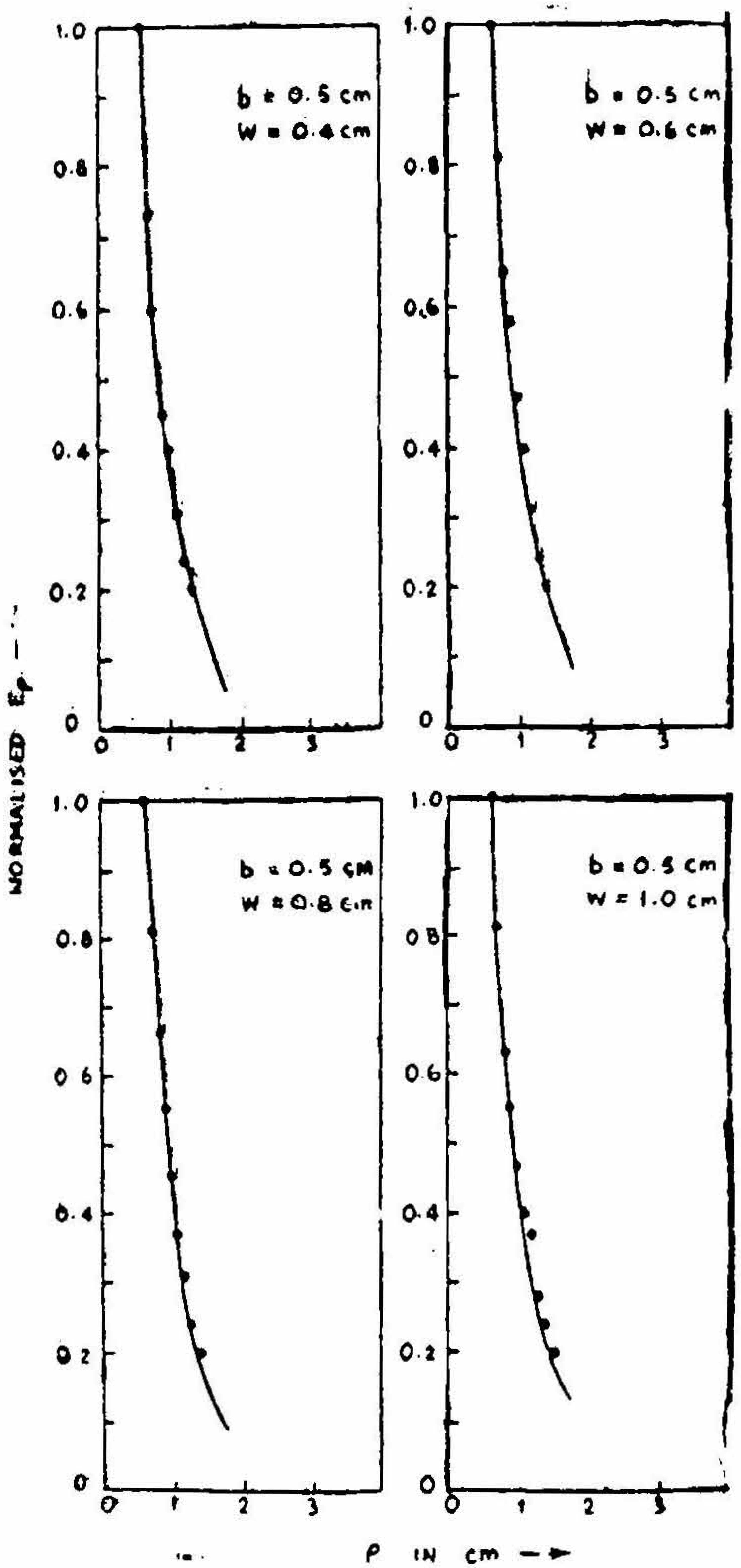

FIG. 5

Experimental and theoretical plots for the component E_ρ

b : Disc-radius —— Theoretical graph

w : Disc-spacing · · Experimental points

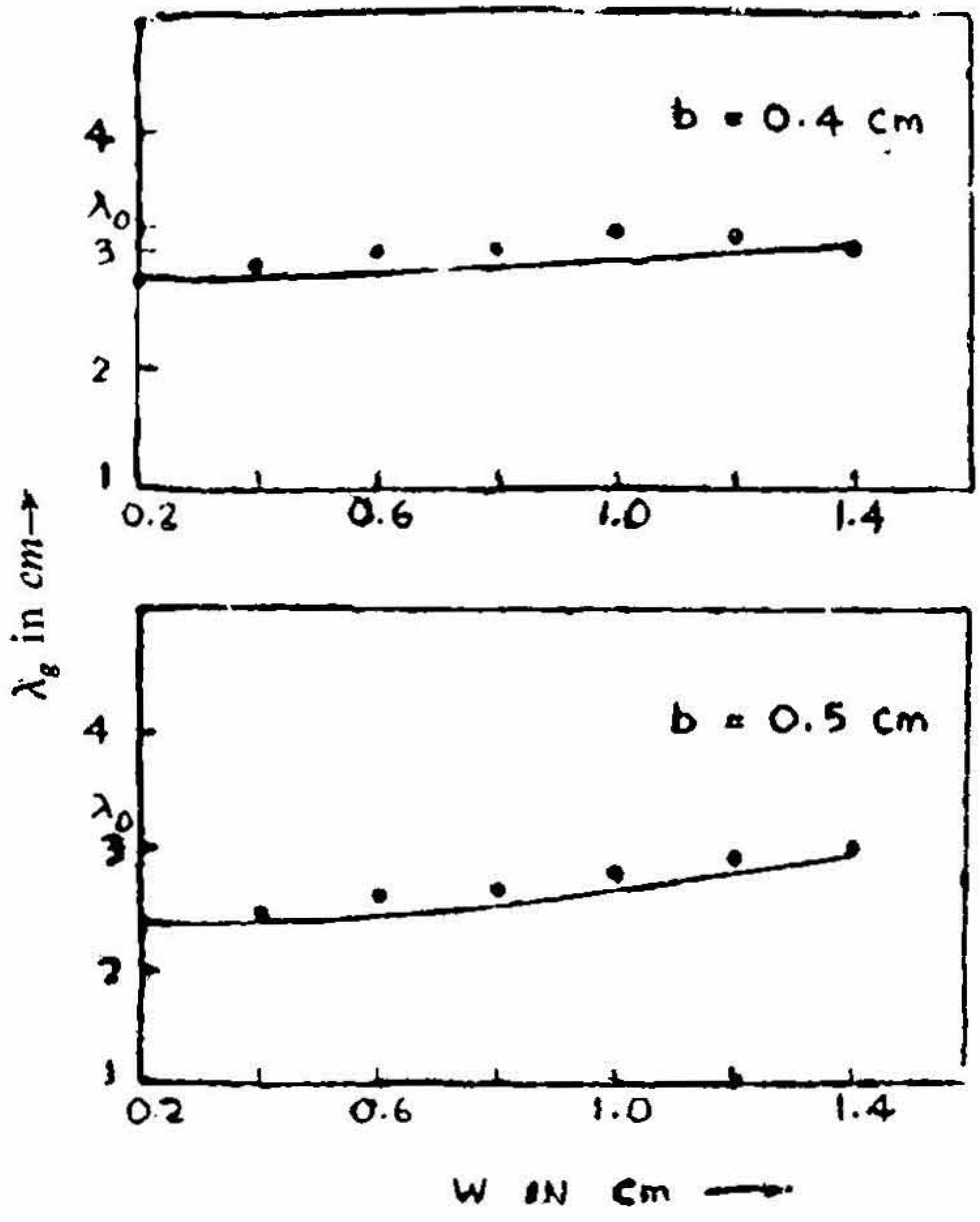

FIG. 6

Theoretical and experimental plots of λg vercus w.

—— Theoretical graph

· · Evperimental points

b : Discc-radius

w ; Disc-spacing

λg: Guide wavelength

5. MEASUREMENT OF RADIATION FIELD

The block schematic diagram (See Fig. 7) shows the arrangement for measuring the radiation field. The method of measurement is conventional. Some of the results of measurement of the power pattern are shown in Figures 8 – 10. The theoretical patterns shown for the sake of comparison are derived from the following relation[2].

$$\vec{E} = D\,\hat{\theta}\left\{\frac{k_0}{\gamma_0}\sin\theta\, K_1(\gamma_0 b)\, J_0(u) + K_0(\gamma_0 b)\, J_1(u)\right\}\frac{\sin X}{x}\cdot\frac{\exp(jk_0 r)}{r} \quad [6]$$

where,

$$X = \frac{(\beta_0 - k_0 \cos \theta) L}{2}$$

$$u = k_0 b \sin \theta$$

and $D = \frac{1}{2} j k_0 C_0 b L \exp(-jX)$

where L is the length of the structure ($=50$ cm.) and θ is the angle measured from the axis of the structure.

Variation of the position of major lobe with disc-spacing W is shown in Fig. 11.

6. DISUSSION OF THEORETICAL AND EXPERIMENTAL RESULTS[1,2].

6·1. *Dispersion Characteristics of the Structure.*

The effect of variation of the frequency of excitation on the propagation characteristics of the structure is determined from the solution of the equation (2). The phase velocity (v_p), group velocity (v_g) are determined from the dispersion diagrams. Some of the values are tabulated in Table 3.

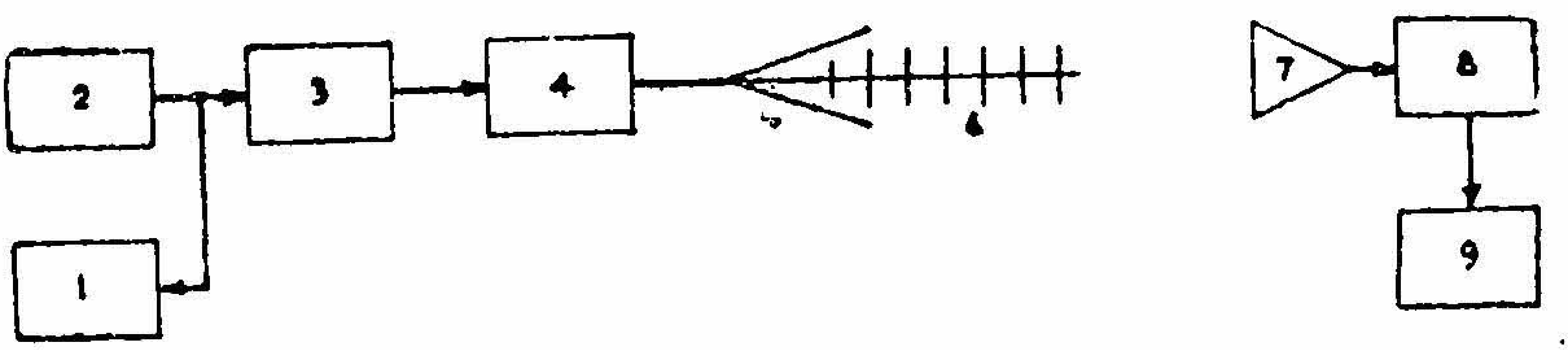

FIG. 7

Black schematic diagram of the expzrimental set-up for radiation field measurement

1. Squire wavc modulator
2. Klystrn power supply
3. Klvstrn (723 A/B) and feed
4. Rectangular waee guid-to-coaxial adapter (Microline Model 249)
5. Circular metal cone
6. Surface wave guide
7. Pyramidal horn
8. Detecting section
9. Detector amplifier

Note : The distance between the feed end of the structure (6) and the horn (7), at any position of the horn is about 2 metres

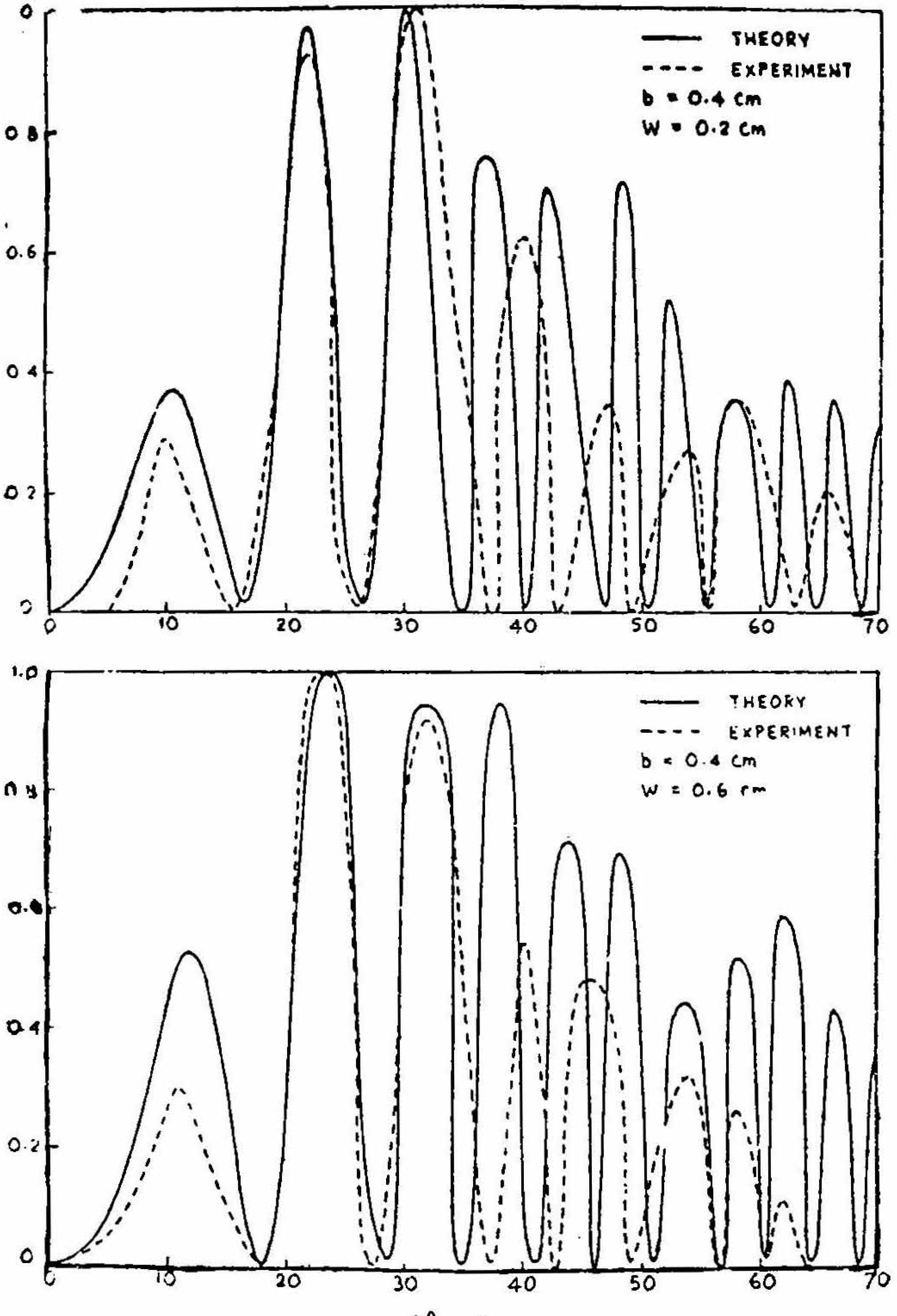

FIG. 8

Experimental and theoretical power patterns

b: Disc-radius w: Disc-spacing

θ: Angle measured from the axis of the structure

length of the structure = 50 *c.m.*

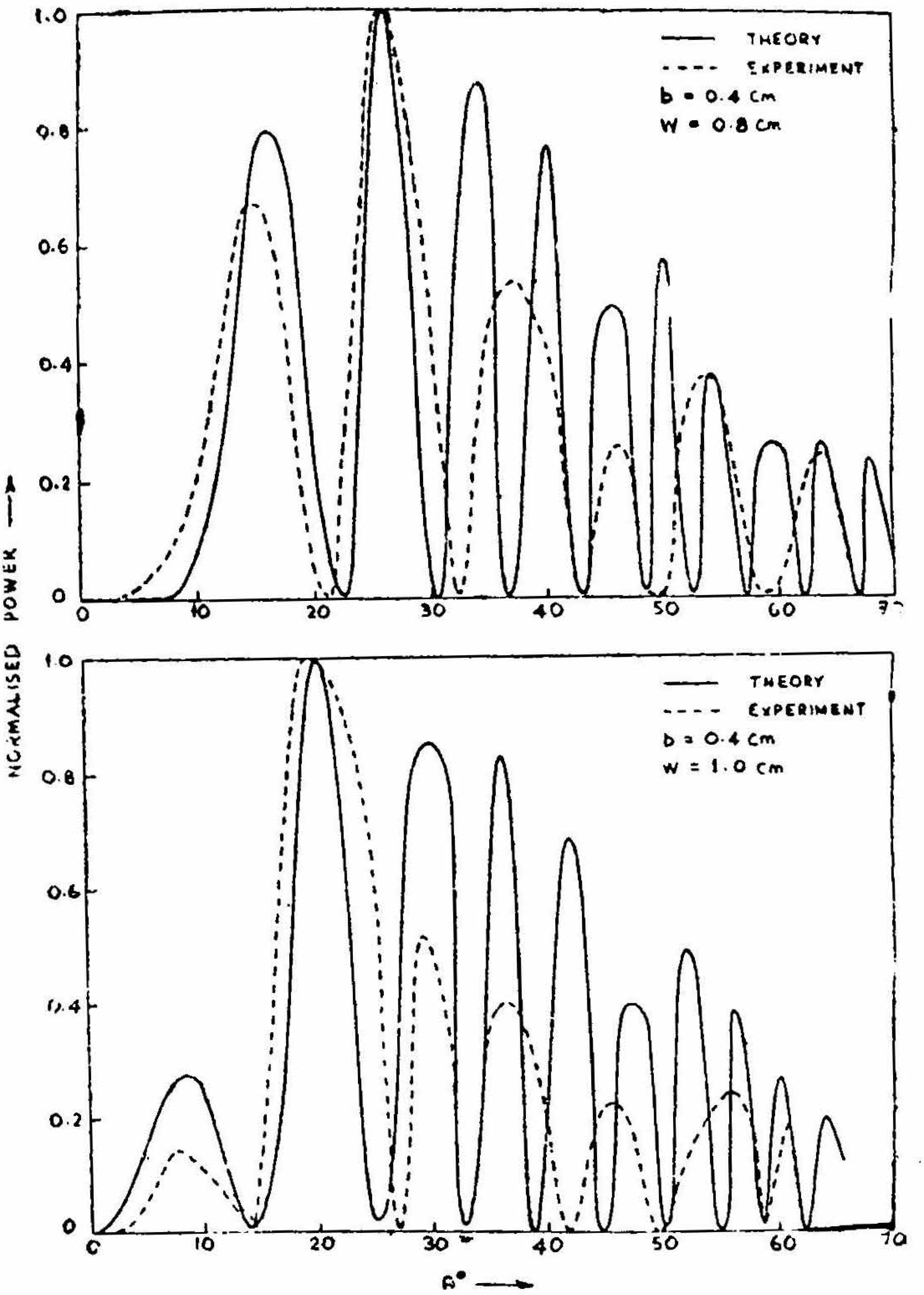

FIG. 9

Experimental and theoretical power patterns

b: Disc-radius w: Disc-spacing

θ: Anglemeasured from the axis of the strucrure, length of the structure = 50 $c.m.$

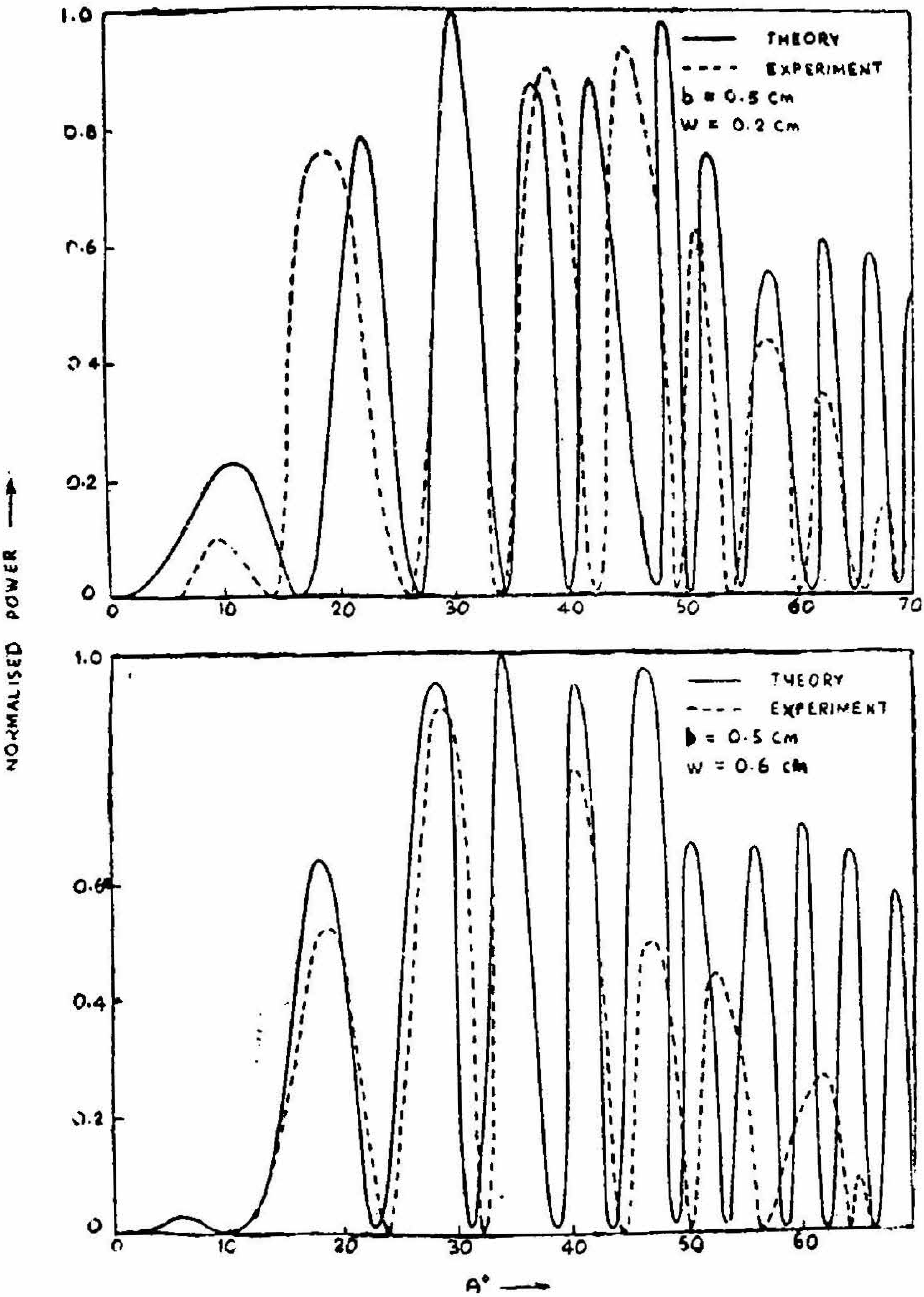

FIG. 10

Experimental and theoretical power patterns

b : Disc-radius *w* : Disc-spacing

θ : Angle measured from the axis of the structure, length of the structure = 50 *c.m.*

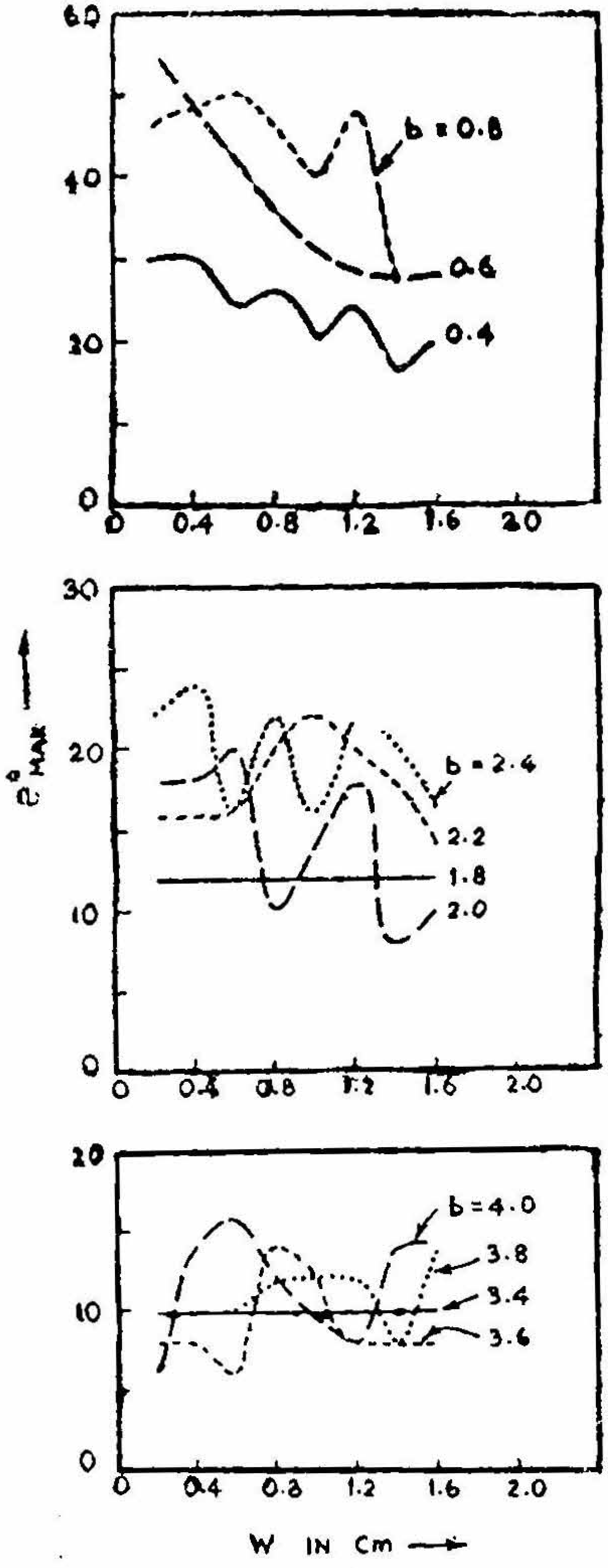

Fig. 11

Plots of the position of the major lobe (in the structure radiation pattern) versus the disc-spacing, W

θ_{Max} : Angle measured from the axis of the structure

b : Disc-spacing in cm

Length of the structure = 50 cm.

TABLE 3

Approximate values of v_p/c, v_g/c and v_pv_g/c^2.

b (cms)	k_0 (radians/cm)	v_p/c	v_g/c	v_pv_g/c^2
0.4	1.6	0.89	0.84	0.75
	4	0.76	0.60	0.45
0.6	1.6	0.67	0.48	0.32
	3,2	0.31	0.05	0.01
0.8	1.2	0.54	0.30	0.16
	1.6	0.38	0.14	0.53
1.8	2.4	0.78	0.27	0.21
	2.8	0.30	0.01	0.003

It follows from the above table that

(i) in any band the phase velocity and group velocity decrease with frequency ; and

(ii) in contrast to the conventional waveguides in which $v_p v_g = c^2$, in this case $v_p v_g < c^2$, and in any band, $v_p v_g/c^2$ decreases with frequency.

6.2 *Attenuation*

The frequency dependence of the attenuation constant (α) of the structure is determined from the relation[1]

$$\alpha = \frac{P_1 + P_2 + P_3}{2lP_t} \qquad [7]$$

where,

$$P_1 = \frac{B^2 \pi^3 W^2 \eta \ (l - W) \ k_0^2 b}{4 \ l^2 \ \gamma_0^2} \ \frac{\epsilon_0}{\mu_0} \ \frac{K_1^2 (\gamma_0 b)}{K_0^2 (\gamma_0 b)} \ J_0^2 (\beta_0 W/2)$$

$$P_2 = \frac{B^2 \pi W \eta}{k_0^2 a} \ \frac{\epsilon_0}{\mu_0} \ \frac{1}{F_0^2 (k_0 b)}$$

$$P_3 = \frac{B^2 \pi^3 \eta}{8 \ F_0^2 (k_0 b)} \ \frac{\epsilon_0}{\mu_0} \left[b^2 \left\{ F_1^2 (k_0 b) - F_0 (k_0 b) \ F_2 (k_0 b) \right\} - \frac{4}{\pi^2 k_0^2} \right]$$

$$P' = \frac{1}{2} B^2 \pi W^2 \beta_0 k_0 \sqrt{\frac{\epsilon_0}{\mu_0}} \frac{G(\gamma_0 b)}{l^2 \gamma_0^4} \left[\frac{J_0(\beta_0 W/2)}{H_0^{(1)}(j\gamma_0 b)} \right]^2$$

$$F_2(k_0 b) = J_0(k_0 a) Y_2(k_0 b) - Y_0(k_0 a) J_2(k_0 b)$$

$$G(\gamma_0 b) = (\gamma_0 b)^2 K_0^2(\gamma_0 b) + 2\gamma_0 b K_0(\gamma_0 b) K_1(\gamma_0 b) - (\gamma_0 b)^2 K_1^2(\gamma_0 b)$$

It is evident that α depends on k_0, or, the frequency (f) in a complicated way and it is difficult to give a definite proportionality relation between α and k_0 from equation (7). It has therefore been thought worth while to make an attempt to derive an approximate relation between α and k_0 from a plot of α versus k_0 made on a log—log scale (See Fig. 12 and 13). The proportionality relation between α and frequency derived from the above figures in different ranges of b and k_0 is tabulated in Table 4.

TABLE 4

Approximate slope $d\alpha / dk_0$ for the plots given in Figures 12 and 13.

b (cm)	k_0 (radians/cm)	$d\alpha / dk_0$	b (cm)	k_0 (radians/cm)	$d\alpha / dk_0$
0.4	1.6	0.82	0.6	2	3.08
	3.2	1.66		2.8	6.69
	4	1.8			
1.8	$2.3 \leq k_0 \leq 2.8$	19.08	2.2	$1.6 \leq k_0 \leq 2$	11.43
	$4.4 \leq k_0 \leq 4.8$	38.19		$3.2 \leq k_0 \leq 3.6$	28.64

It is observed that (a) on the average α is proportional to $f^{7/5}$ and that α increases very rapidly with f for $b = 1.8$ and 2.2 cms, and (b) the proportionality factor for f increases with f for $b = 0.4$ and 0.6 cms.

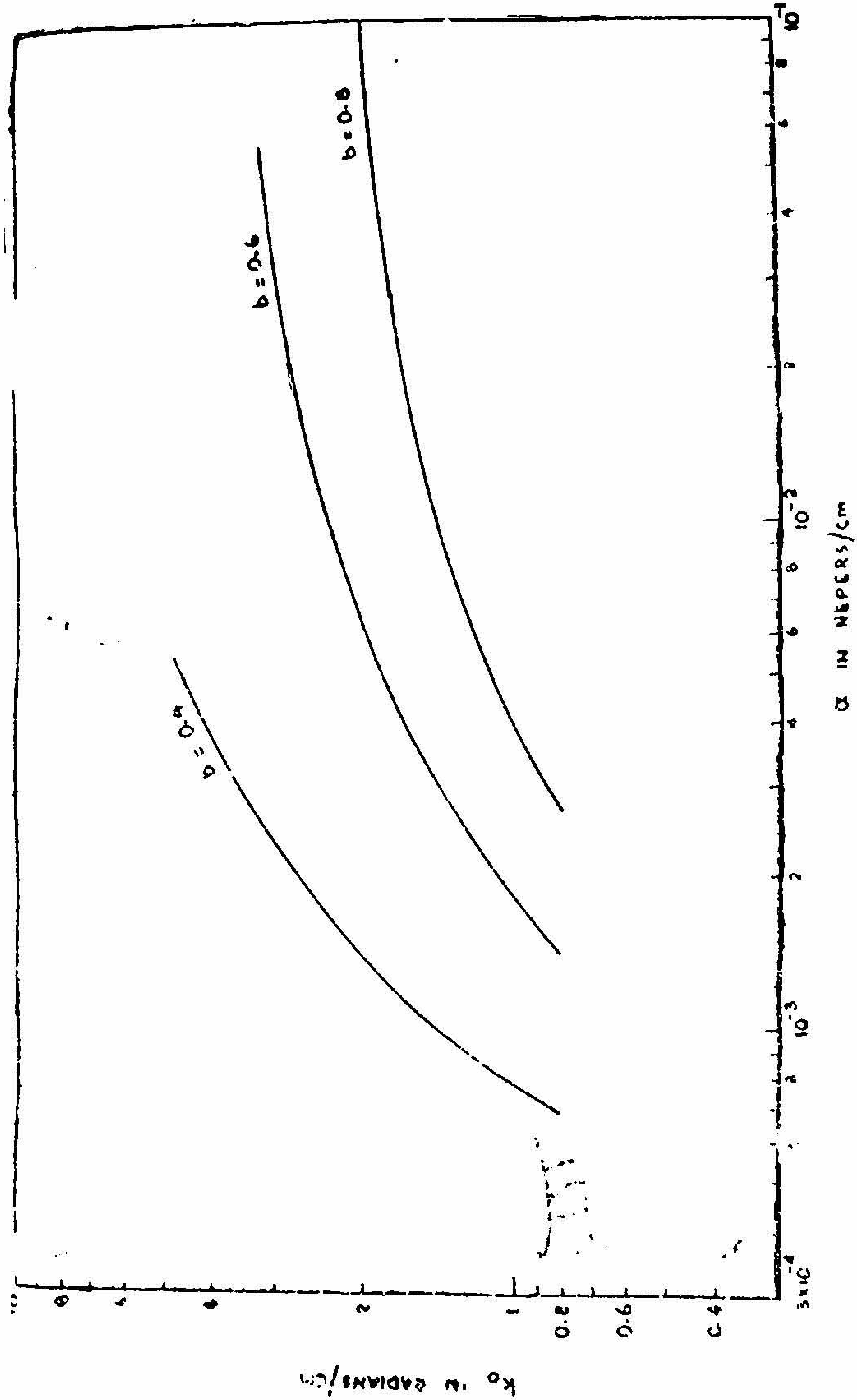

FIG. 12

Plots of k_0 versus α

k_0 : Free space wave number b : Disc-radius in *c.m.*
α : Attenuation constant Disc-spacing = 0.2 *c.m.*

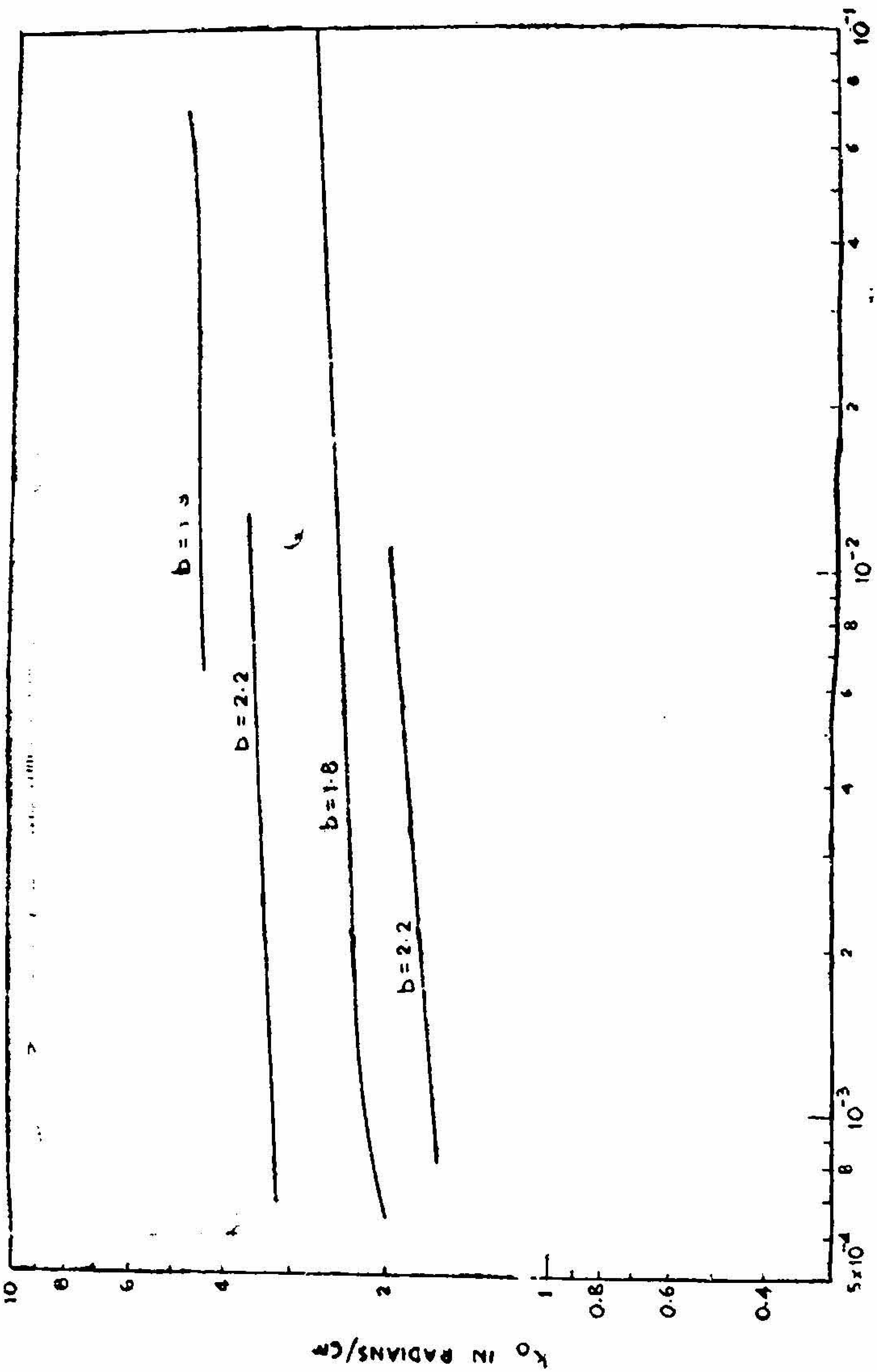

FIG. 13

Plots of k_0 versur α

Free space wave number b : Disc-radius in *c.m.*

Attenuotion constant Disc-spacing = 0.2 *c.m.*

6.3 *Purity of Surface Wave.*

The close agreement between theory and experiment for the radial field decay (See Figs. 3-5) and guide wavelength (See Fig. 6) indicates that the surface wave launched on the structure is pure for the values of b and W indicated in the figures.

6.4 *Impedance of the Grooves.*

The condition under which the structure can support a pure surface wave can also be considered from the point of view of groove impedance. The impedance of the grooves is given by the relation

$$\frac{E_z^{(2)}}{H_\phi^{(2)}} = -j\left(\sqrt{\frac{\mu_0}{\epsilon_0}}\right)\frac{F_0(k_0 b)}{F_1(k_0 b)} \qquad [8]$$

It has been pointed out in an earlier paper[1] published elsewhere, that surface wave roots can exist when

$$\frac{F_1(k_0 b)}{F_0(k_0 b)} < 0 \text{ or, } \frac{F_1(k_0 b)}{F_0(k_0 b)} > 0, \text{ but}$$

very small. This means that the surface wave roots can exist when the impedance of the grooves is inductive or is capacitive but very high.

6.5. *Launching Efficiency*

The question of how effectively surface wave can be launched on a structure depends not only on the nature of the surface of the structure but also on the launching efficiency of the launching device which in the present case is a slot of radius h. The launching efficiency η_e is given by the relations[2]

$$\eta_e = \frac{P_S}{P_R + P_S} \qquad [9]$$

where,

$$P_S = \frac{32\, e^{-2} h^2 \gamma_0}{b^2 \beta_0 G(\gamma_0 b)} \frac{\pi}{\gamma_0^2} \frac{\omega \mu_0 \gamma_0}{k_0^2} (b\,\gamma_0)^2 K_1^2(\gamma_0 h)$$

$$P_R = 4\pi\, e^{-2} h^2 Z_0 \int_0^{\pi/2} |\bar{G}(\theta)|^2 \sin\theta \, d\theta$$

$$\bar{G}(\theta) = F(-k_0 b \sin\theta)\; H_1^{(1)}(-k_0 h \sin\theta) + H_1^{(2)}(-k_0 h \sin\theta)$$

$$F(-k_0 h \sin 0) = [x_S k_0^2 H_1^{(2)}(-k_0 b \sin\theta) - \omega \mu_0 k_0 \sin\theta\, H_0^{(2)}(-k_0 b \sin\theta)] / [\omega \mu_0 k_0 \sin\theta\, H_0^{(1)}(-k_0 b \sin\theta) - X_S k_0^2 H_1^{(1)}(-k_0 b \sin\theta)]$$

$$X_S = \frac{\omega \mu_0 \gamma_0}{k_0^2} \frac{K_0(\gamma_0 b)}{K_1(\gamma_0 b)}$$

$$\tilde{e} = \frac{V k_0^2}{4 \omega \mu_0}$$

The launching efficiency depends on b, w and h. It is difficult to determine the sensitivity of η_e with respect to these parameters. It is however, observed from the plots of maximum η_e versus b and W (See Figures 14 and 15) that maximum η_e is more sensitive with respect to b than W. The following table contains some typical values of maximum launching efficiency and the corresponding values b, W, c/v_p and ,

TABLE 5

Maximum value of η_e and corresponding values of c/v_p and λ_g

b(cm)	W(cm)	λ_g(cm)	c/v_p	η_e(%)
0.4	0.8	2.85	1.12	97
	1.2	2.98	1.07	94
	1.6	3.09	1.03	88
1.8	0.8	3.19	1	43
	1.2	3.12	1	40
	1.6	3.2	1	35
2	0.8	2.95	1.08	97
	1.2	3.06	1.05	92
	1.6	3.14	1.02	78
3.6	0.8	2.98	1.07	94
	1.2	3 07	1.04	89
	1.6	3.15	1.01	78

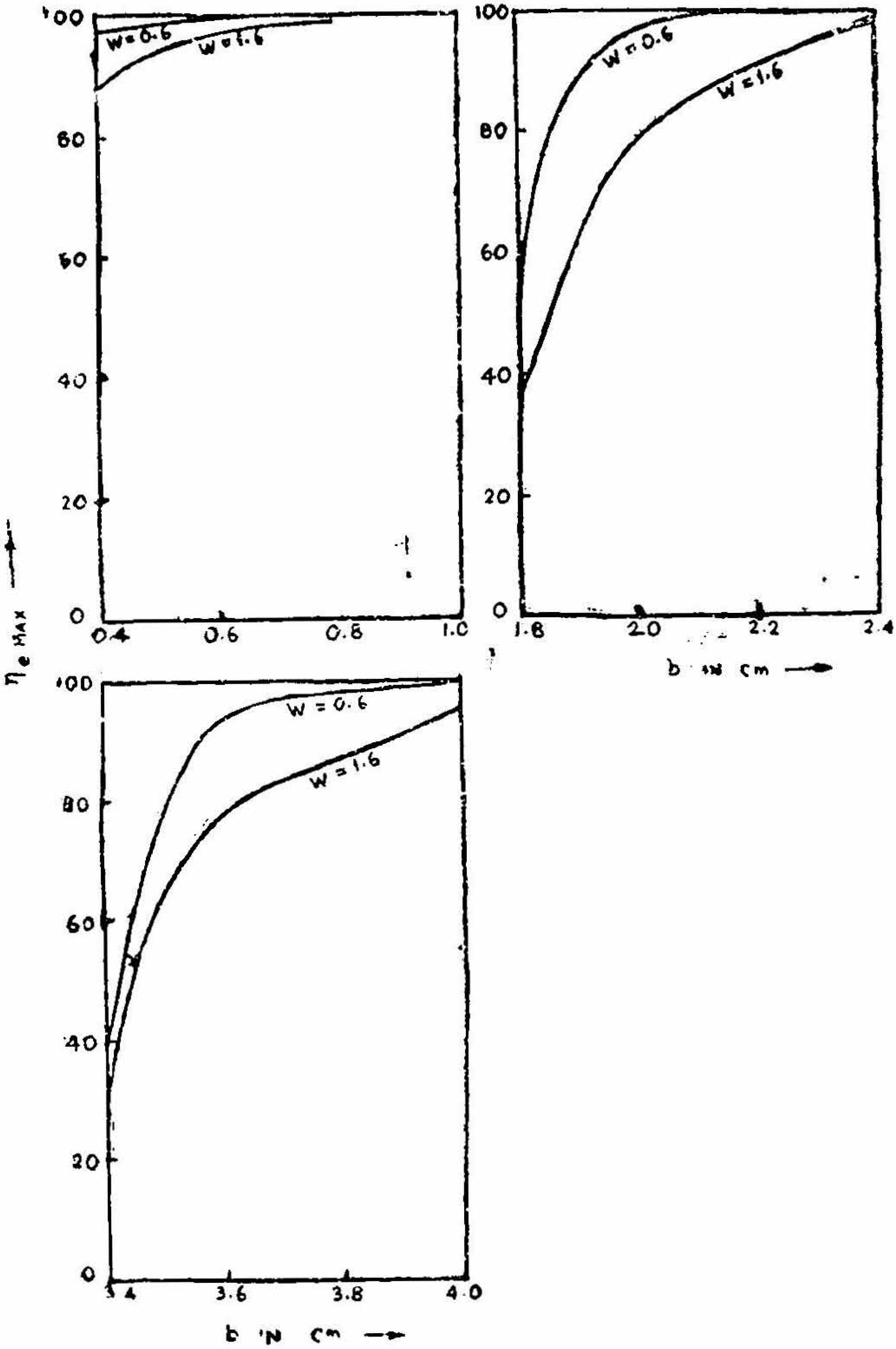

FIG. 14

Plots of maximum launching efficiency versus *b*.

b : Disc-radius.

W : Disc-spacing in cm.

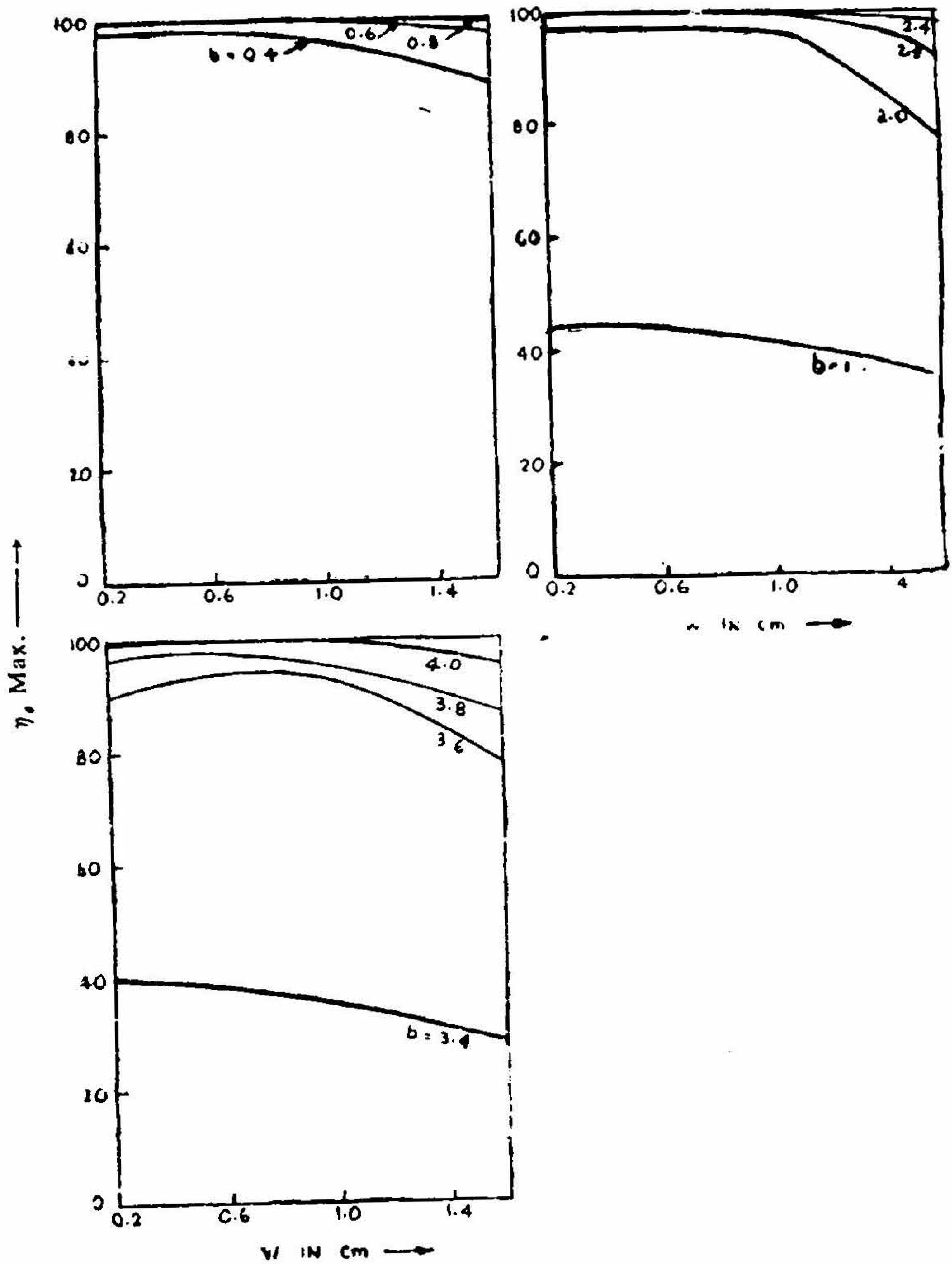

Fig. 15

Plots maximum launching efficiency versus w.

b: Disc-radius in cm.

w: Disc-spacing.

6.6 *Source-excited Radiation Field.*

The radiation field is not only due to structure radiation but also due to the presence of the exciting source. The source field modified by the structure is given by[2],

$$H_\phi\,(\text{rad}) = -\frac{2\,j\,\bar{c}\,h\,G\,(\theta)}{r}\exp\,(-j\,k_0\,r)$$

is determined for the case (i) when b and W are such that it supports surface waves (class I), (ii) when b and W are such that it does not support surface wave (class II). A plot of the position of the major lobe versus the disc-radius is given in Fig. 16 from which it follows that the radiation pattern changes from nearly end fire to broadside direction and from broadside to end fire direction as the disc-radius is increased in class I and II respectively.

6.7 *Comparison between Disc-loaded structure, Sommerfeld line and Harms-Goubau line*

In order to compare the surface wave characteristics of the corrugatad line with that of the Harms-Goubau line, the thickness of the polythene coating of the latter which would give the same phase velocity as that of the corrugated structure is found. The radius b' of the dielectric coating of the Goubau line is determined from the following relation[3],

$$\frac{F_0\,(\gamma_i\,b')}{F_1\,(\gamma_i\,b')} = -\left(\frac{k_i}{k_0}\right)^2\frac{\gamma_0}{\gamma_i}\;\frac{K_0\,(\gamma_0\,b)}{K_1\,(\gamma_0\,b)} \qquad [10]$$

where, $k_i^2 = \omega^2\,\mu_0\,\epsilon_i\,,\quad \gamma_i^2 = k_i^2 - \beta_0^2$

$$F_r\,(\gamma_i\,b') = J_0\,(\gamma_i\,a)\;Y_r\,(\gamma_i\,b') - Y_0\,(\gamma_i\,a)\;J_r\,(\gamma_i\,b')$$

where, $r = 0,\ 1.$

ϵ_i is the dielectric constant of the polythene, γ_0 is the radial propagation constant for the fundamental harmonic and b is the disc-radius of the equivalent structure.

The value of b' which would give the same phase velocity corresponding to particular values of b and W of the corrugated line is calculated from equation [10] and the results are given in Table 6. The blank spaces in the table correspond to the case $\beta_0 < k_i$. Since physically $\beta_0 > k_i$, it follows that b' cannot be determined for values of b and W for which $\beta_0 < k_i$. It is observed that when $b \approx a$, $b' > b$.

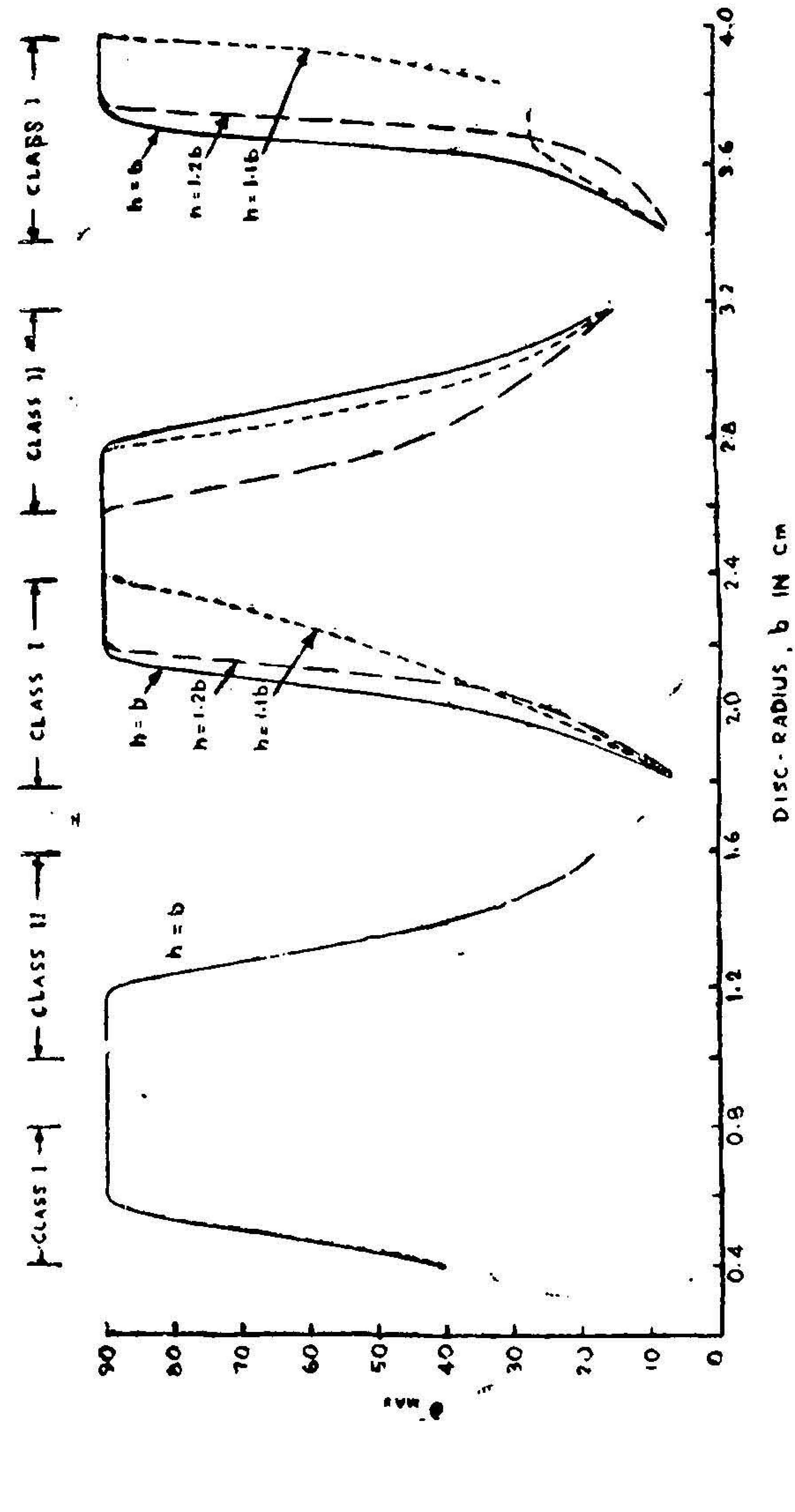

FIG. 16

Plots of the position of the major lobe (in the source excited radiation pattern) versus the disc-radius.

θ_{Max} : Angles measured from the axis of the structure

h : Slot-radius.

Disc-spacinp=0.2 cm.

TABLE 6

Values of b' (cm) and the corresponding b and W.

W (cm)	.2	.4	.6	.8	1.0	1.2	1.4	1.6
b (cm)								
0·4	·495	·51	·485	·46	·43	·39	·36	·33
0·6	–	–	–	1·165	·785	·64	·54	·475
0·8	–	–	–	–	–	–	1·205	6·755
1·8	·27	·265	·265	·26	·26	·26	·26	·255
2·0	·51	·515	·495	·48	·45	·415	·37	·35
2·2	1·38	1·405	·975	·785	·67	·58	·51	·455
2·4	–	–	–	–	–	1·115	·765	·63
3·4	·28	·28	·28	·275	·275	·27	·27	·265
3·6	·505	·525	·505	·48	·455	·42	·38	·35
3·8	1·1	1·105	·89	·745	·65	·57	·51	·455
4	–	–	–	–	–	·985	·73	·6

The attenuation constant calculated as a function of b and W with the aid of equation (7) is compared with the attenuation constant of the equivalent Harms-Gouban line in Table 7.

TABLE 7

Values of α for Harms-Goubau and corrugated surface wave line

W (cms)	b (cms)	b' (cm)	γ_0 radians/cm	α (H.G.) aepers/cm	α (corrugated) nepers/cm
1.6	0.4	0.33	0.525	1.1×10^{-4}	0.43×10^{-4}
0.2	1.8	0.27	0.111	0.44×10^{-4}	0.56×10^{-4}
1.6	1.8	0.255	0.059	0.35×10^{-4}	0.65×10^{-4}
0.2	3.4	0.28	0.125	0.46×10^{-1}	0.84×10^{-4}
1.6	3.4	0.265	0.063	0.35×10^{-4}	0.64×10^{-4}

The loss (L') per 100 ft. of Harms-Goubau line is given by[3]

$$L' = \frac{P(\gamma_0 b')}{b(\lambda_0)^{1/2}} + \frac{\epsilon_0}{\epsilon_i - \epsilon_0} \tan\delta \frac{\lambda_0}{b'^2} Q(\gamma_0 b')\ (db)$$

$$P(\gamma_0 b') = -1.33 \times 10^4 (\epsilon_0/\mu_0)^{1/4} \left(\frac{\pi}{\sigma}\right)^{1/2} \frac{1}{ln\ \gamma_0 b' + 0.38} \qquad [11]$$

$$Q(\gamma_0 b') = 2.11 \times 10^3 \left(1 - \frac{0.5}{ln\ \gamma_0 b' + 0.38}\right)(\gamma_0 b')^2$$

σ : Conductivity of the inner conductor.

$\tan\delta$: Loss tangent of the dielectric.

The radial propagation constant γ_S, delay-ratio $(c/v_p)_S$ and the attenuation constant α_S of the Sommerfeld surface wave line of radius 'a' are as follows

$$\gamma_S = 0.01 \text{ radians/cm}$$

$$(c/v_p)_S = 0.001$$

$$\alpha_S = 0.2 \times 10^{-2} \text{ nepers per cm.}$$

The above values for Sommerfeld line are calculated from the following relation[3].

$$\xi\ ln\ \xi = \eta$$

$$\xi = (-j\ 0.89\ \gamma_S a)^2$$

$$\eta = 2\ (0.89)^2\ [k_0^2 a / |k_c|] \exp(j\ 3\pi/4)$$

$$k_c = (\omega \mu_0 \sigma)^{1/2} \exp(-j\pi/4) \qquad [12]$$

CONCLUSION

(i) The groved structure supports a surface wave when the impedance of the grooves is inductive[3], and also when the impedance is capacitive but very high.

(ii) For the maximum value of disc-radius b, in the range in which a surface wave root exists, the launching efficiency is very high and the radiation pattern is broadside.

(iii) For the maximum value of b in the range in which surface wave root exists, the launching efficiency is very poor and the radiation pattern is near end fire.

(iv) The structure radiation pattern consists of a large number of lobes. In some cases, the minor lobe levels are comparable with that of the major lobe.

(v) When the structure is excited by a magnetic ring source in TM_0-mode, the source-excited radiation field pattern depends mainly on the magnitude of the surface impedance and not on its nature[2].

8. REFERENCES

1. (Miss) H. M. Girija, S. K. Chatterjee .. .. *J. Ind. Inst. Sci.*, 53, 269, 1971
2. ———— .. .. *Indian J. Pure Appl. Physics* (Uuder publication)
3. Gorban .. .. *J. Appl. Phys*, 21, 1119, 1950.